SCIENTIFIC REPORTS
nature research

OPEN

Polaron Diffusion in Pentathienoacene Crystals

Marcelo Lopes Pereira[1], Rafael Timóteo Sousa[2], William Ferreira Giozza[2] & Luiz Antonio Ribeiro[1]✉

Molecular crystals have been used as prototypes for studying the energetic and dynamic properties of charge carriers in organic electronics. The growing interest in oligoacenes and fused-ring oligothiophenes in the last two decades is due, in particular, to the success achieved in conceiving pentacene-based organic photovoltaic devices. In the present work, a one-dimensional Holstein-Peierls model is designed to study the temperature-dependent polaron transport in pentathienoacene (PTA) lattices. The tight-binding Hamiltonian employed here takes into account intra and intermolecular electron-lattice interactions. Results reveal that polarons in PTAs can be stable structures even at high temperatures, about 400 K. During the dynamical process, these charge carriers present a typical 1D random walk diffusive motion with a low activation energy of 13 meV and a room temperature diffusivity constant of 1.07×10^{-3} cm^2 s^{-1}. Importantly, these critical values for the polaron diffusion and activation energy are related to the choice of model parameters, which are adopted to describe pristine lattices.

Organic crystalline semiconductors have emerged in the last two decades as promising solutions in substituting Silicon and Gallium for the manufacture of electronic devices, especially those aimed to capture, emit, and control light[1–5]. Among the reasons for that stand out their lower environmental impact, good transparency, and flexibility[6,7]. Particularly, molecular crystals present two types of electron-phonon (e–ph) interactions, namely local intramolecular (Holstein-type) and non-local intermolecular (Peierls-type) interactions[8–10]. The Holstein-type[11,12] is related to covalent bonds and modulates the site energy vibrations, and the Peierls-type, in turn, describes the modulation of the intermolecular vibrations governed by weak van der Waals interactions[13]. In these materials, polarons are the primary structures that play the role of the charge transporter[9,14].

Recently, Zhang and colleagues have theoretically investigated the charge transport parameters and carrier mobilities in pentacene and pentathienoacene (PTA) crystals within the framework of Marcus' semi-classical theory and quantum nuclear tunneling model, coupled with random walk simulation[15]. In their work, a systematic comparative study was also carried out for pentacene and PTA to gain insights into the theoretical design of these materials. The key finding in their results have revealed that pentacene and PTA present similar lattice structures, but they exhibit substantially different intrinsic transport properties. By using a similar approach, Takimiya *et al.* studied several high-mobility organic semiconductors (among them the PTA) to obtain their molecular factors and electronic structure, which would benefit the design strategies for the synthesis of molecules for new field-effect applications[16]. In an overall fashion, their results suggest that molecular design strategies should be based on the understanding of intermolecular orbital overlaps and their dimensionality in the crystal. Importantly, other relevant works have also used similar methods to study the diffusion of charge carriers and excitons in organic materials[17–24]. Albeit several works have used a quantum-mechanical description to describe the polaron dynamics[25–30], a coherent quantum-mechanical description of polaron diffusion in PTA is still missing.

In the present work, we extend our very recent analysis of polaron properties in PTA[31] by investigating its temperature-dependent dynamics in this class of material. The numerical approach employed here is based on a Holstein-Peierls Hamiltonian that takes into account both intra and intermolecular electron-lattice interactions to consider the presence of a polaron in a one-dimensional PTA lattice. We systematically investigate the impact of different thermal bath regimes on polaron stability and dynamics. In this sense, our results give information about diffusion parameters such as diffusion length, diffusivity, activation energy, as well as charge mobilities.

[1]Institute of Physics, University of Brasília, Brasília, 70919-970, Brazil. [2]Department of Electrical Engineering, University of Brasília, Brasília, 70919-970, Brazil. ✉e-mail: ribeirojr@unb.br

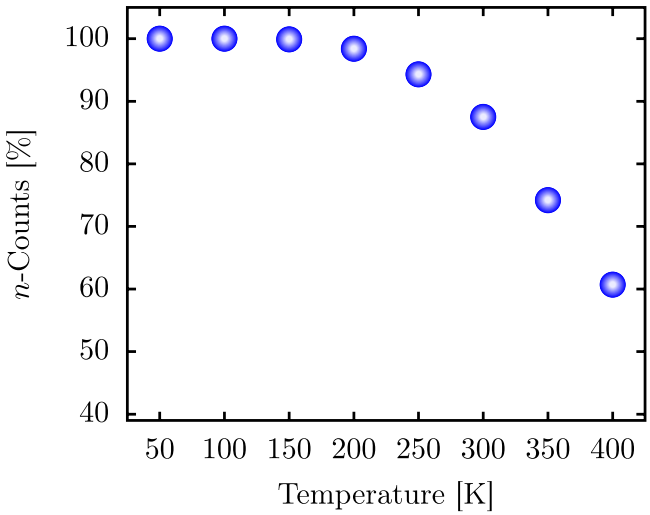

Figure 1. Temperature-dependent stability of large polarons in model 1D PTA lattices. The n-counts stands for the counting of stable polarons based on $\overline{\text{IPR}}$ measurements.

Results

To characterize the polaron diffusion in PTA crystals, we adopt a one-dimensional lattice with 100 sites. The system dynamics take place during 5 ps for temperature regimes ranging from 50 to 400 K, with an increment of 50 K and 1000 realizations for each one of them. All the realizations start from the same initial state, a stable polaron on its ground state configuration[31]. Here, we use two measures to characterize the polaron stability: the polaron formation energy (E_P) and the inverse participation ratio (IPR) related to the system's charge density. E_P is the energy difference between the neutral ground state and relaxed confirmation ($E^{\pm}$) energies in the presence of additional charge. In this sense, once the ground state and relaxed energies for a PTA lattice are obtained, the polaron formation energy is calculated as $E_P = J_0 - E^{\pm}$, where J_0 is the transfer integral between next-neighboring molecules in a pristine lattice[13]. For a lattice with $J_0 > 0$, stable polarons take place when $E_P < 0$. We obtain $E_P = -39$ meV for a 1D PTA lattice, that agrees with values reported for other molecular crystals, that are about 100 meV or less[32,33]. It is worthwhile to stress that $E_P \sim J_0$ denotes a Fröhlich-like polaron solution[34] (or large polaron)[34], whereas $E_P \gg J_0$ stands for the Holstein-like polaron solution (or small polaron)[11]. As discussed in our previous researches, large polarons are dynamically stable and should be considered the primary quasiparticles when it comes to the charge transport mechanism in organic crystalline semiconductors[31,35–37].

The IPR, in turn, is the quantity that measures how many sites share the additional charge, so that $0 < \text{IPR} < 1$, and is given by

$$\text{IPR} = \frac{\sum_j |\rho_j|^2}{(\sum_j |\rho_j|^2)^2}, \tag{1}$$

where ρ_j is the charge density of j site. The IPR related to a large polaron solution in a 2D PTA lattice may vary from 0.35 to 0.70 and the configuration of its ground state geometry was presented in our previous research[31]. For the 1D PTA lattice as modeled here, we obtain IPR = 0.40 that characterizes a stable large polaron.

Having presented the initial condition of the simulations, we now present the main features of the polaron diffusion in 1D PTA lattices. To do so, we begin by discussing the impact of the temperature on the polaron stability in these materials. Figure 1 depicts the counting of stable polarons (n-counts) for a given thermal bath having as reference the average of IPR ($\overline{\text{IPR}}$). The $\overline{\text{IPR}}$ is calculated using the IPR values obtained at each time step during the last 2 ps, neglecting, therefore, the initial polaron configuration that is the same for all realizations. As mentioned above, we count just stable large polarons, and they present IPR values ranging from 0.35 to 0.70. In this sense, Fig. 1 illustrates the percentage count of stable polarons over 1000 realizations in which $\overline{\text{IPR}}$ lies in the range mentioned above for different thermal baths ranging in the interval 50–400 K with an increment of 50 K. From this figure, we can rapidly note that polarons tend to be less stable structures for temperatures higher than 150 K.

For thermal baths above this critical value, a considerable part of the energy related to the molecular vibrations, that are imposed by thermal random forces, is transferred to electrons. This mechanism of energy transfer between lattice and electrons takes place because of intra and intermolecular e-ph interactions. If this transfer continues unhindered, the charge decouples from the lattice and the composite state between charge and lattice deformations, which characterized the polaron, vanishes resulting in the dissociation of this quasiparticle.

For temperatures between 200 and 300 K, the polaron dissociates in few realizations so that more than 80% of them result in stable large polarons. For thermal baths between 300 and 400 K, more than 60% of realizations result in stable charge carriers, which suggests that polarons can be stable structures at room temperature regimes when it comes to 1D PTA lattices.

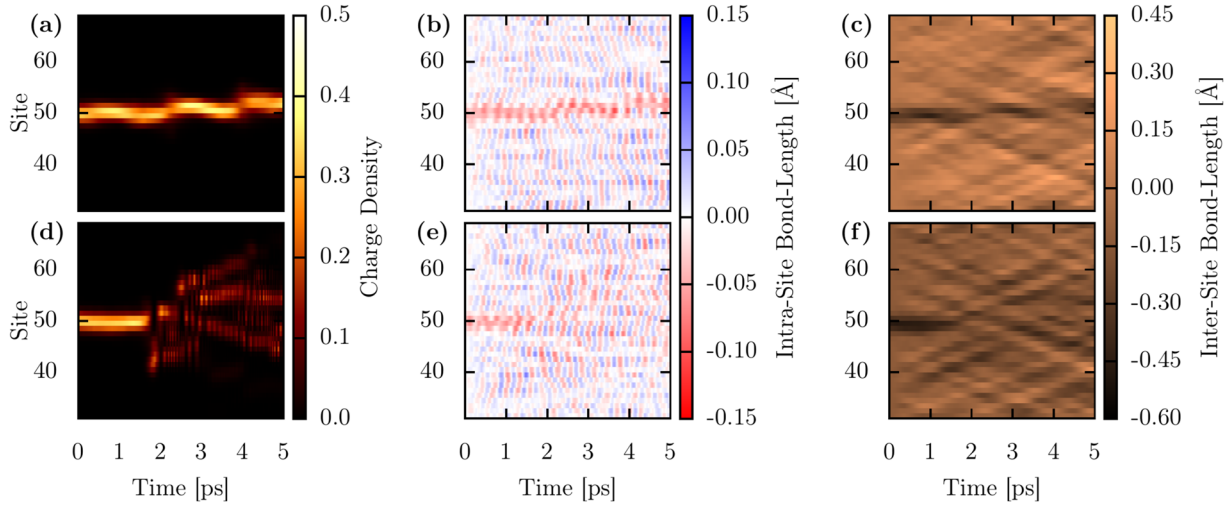

Figure 2. Polaron dynamics in a model 1D PTA lattice. Panels (a,d) depict the temporal evolution of the mean charge density, (**b,e**) and (**c,f**) show the temporal evolution for the intra (u_j) and intermolecular (v_j) displacements, respectively.

The trend for the temperature-dependent polaron motion in model 1D PTA lattices can be summarized in Fig. 2. Figure 2(a–f) illustrate the polaron dynamics for 150 K and 250 K, respectively. Particularly, Fig. 2(a,d) show the temporal evolution of the mean charge density, Fig. 2(b,e) and Fig. 2(c,f) depict the temporal evolution for the intra (u_j) and intermolecular (v_j) displacements, respectively. In Fig. 2(a) one can see that the molecular charge, initially centered at site 50, performs a random motion going back and forth among the lattice sites 50–53. The intra and intermolecular molecular vibrations impose such a random walk motion presented by the molecular charge. In Fig. 2(b), one can realize that there are localized red regions that follow the movement of the molecular charge. These regions denote local intramolecular compressions that are associated with the presence of the additional charge that forms the polaron. The apparent roughness in Fig. 2(b) illustrates how the intramolecular vibrations for the rest of the lattice behave during the time. Analogously, in Fig. 2(c), there are local black regions following the motion of the molecular charge. These distinct regions are local intermolecular compressions associated with the presence of a polaron in the lattice. It is clearly shown by Fig. 2(b,c) that the intra and intermolecular local deformations follow the motion of the molecular charge until the end of the simulations. This collective behavior between charge and lattice deformation presented during the system dynamics represents how the polaron can keep its integrity for small temperature regimes. A different case for the physical picture discussed above can be seen in Fig. 2(d–f), that shows the system dynamics for 250 K. In Fig. 2(d) it is possible to note that the initial sign for the charge localization that denotes the formation of a stable polaron breaks at 2 ps spreading charge through the lattice. From that moment, the charge decouples from the lattice and the local intra, and intermolecular compressions vanish, and a stable polaron is not present in this particular realization.

The overall description of the polaron diffusion in PTA lattices can be achieved by studying an ensemble of its trajectories for a given thermal bath. In this sense, Fig. 3 illustrates the counting for the final position of the polaron (Fig. 3(a)) and its propagation (Fig. 3(b)) for 1000 realizations at 50 K. Figure 3(a) shows the polaron distribution regarding the distance from the origin (site 50) during 5 ps of simulation. Each bar Fig. 3(a) denotes the final position counting for the polaron, used to understand the critical limit for its diffusion in a PTA lattice. The bars are centered in molecules nearby the central unit in which the polaronic charge is placed, as represented in the bottom of Fig. 3. The Gaussian regression denotes that the average position for the polaron displacement is zero. This analysis can be used to derive the probability of finding a polaron at a region in the lattice for a certain thermal bath. The lines in Fig. 3(b) represent the polaron position as a function of time for a given realization. The polaron trajectory ($x_p(t)$) is obtained by using the expression

$$x_p(t) = \frac{n}{2\pi}\arg\left(\sum_{l=1}^{n}\exp\left(\frac{2\pi i l}{n}\right)\times\bar{\rho}(t)\right)\times a, \tag{2}$$

where n is the total number of molecules, and a is the lattice constant[38]. Here, we set $a = 3.5$ Å. One can note that the polaron performs a typical Brownian motion. As mentioned above, the fluctuations in the polaron trajectory are imposed by the temperature effects. Moreover, one can see that there is a dispersion trend of the polaron path, suggesting a diffusive behavior.

Figure 4 shows how the temperature regimes used here impact the polaron diffusion in model 1D PTA lattices. In this figure, we can note that for higher temperatures, the polaron displacement from its origin increases. Accordingly, the counting for the zero displacement decreases proportionally. These results suggest that the temperature-dependent polaron transport in PTA lattices is limited to around twelve molecules. Importantly, the model system used here is a pristine lattice. Therefore, this critical limit for the polaron diffusion in real systems

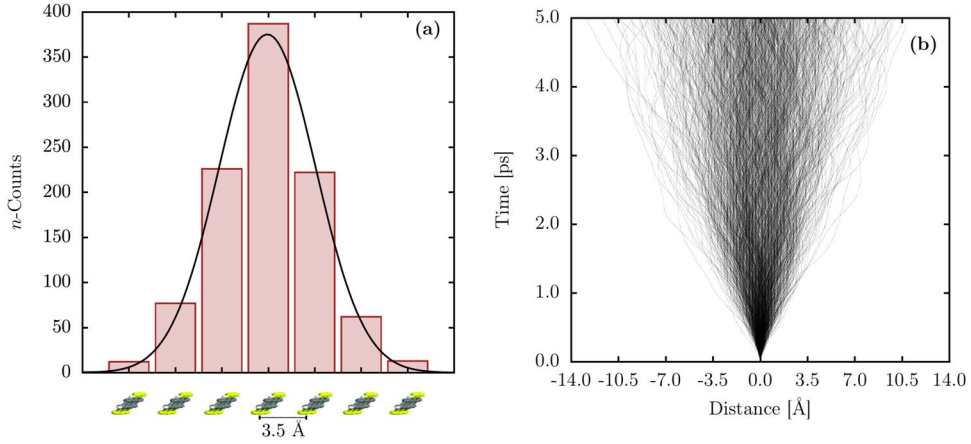

Figure 3. (**a**) Distribution of the of the polaron displacement regarding its initial position at 5 ps for 50 K. (**b**) Polaron trajectory for 1000 realizations.

should be, in fact, substantially smaller due to, for instance, lattice defects and charge recombination that can reduce the mean free path of charge carriers in organic semiconductors[39,40].

Now we can turn to the discussions about the polaron mobility in PTA lattices subjected to a thermal bath. To do so, Fig. 5(a)depicts the time evolution of the mean-square displacement for the polaron trajectories ($x_p^2(t)$) presented in Fig. 3(b). The inset panel, Fig. 5(b), shows the regression for the temperature-dependent polaron diffusivity. The red dashed line in Fig. 5(a) establishes the linear regression over 1000 realizations. The angular coefficient of this regression stands the polaron diffusion according to the following expression

$$D = \frac{1}{2N}\lim_{t\to\infty}\frac{\left\langle x_p^2(t)\right\rangle}{t}, \tag{3}$$

where N is the system's dimensionality. In addition, the obtained diffusion values are used to estimate the polaron mobility, μ, by using the Einstein relationship

$$\mu = \frac{e}{k_B T}D, \tag{4}$$

where e is the electronic charge, k_B is the Boltzmann's constant, and T the temperature. The temperature-dependent polaron transport in organic crystalline semiconductors follows an Arrhenius type law

$$D(T) = D_0 \exp(-E_A/k_B T), \tag{5}$$

where D_0 is the maximum diffusion coefficient, and E_A is the activation energy for the diffusion. As represented in Fig. 5(b), we have performed a regression to derive the polaron diffusivity. The values obtained are $D_0 = 1.07 \times 10^{-3}$ cm^{2}s^{-1} and $E_A = 13.08$ meV. Furthermore, one can note in Fig. 5(b) that the diffusion (D) increases for higher temperature values. Importantly, the calculated D_0 is in the same order of magnitude of values reported in the literature for other organic crystalline systems[41]. We obtain a small value for the activation energy as a consequence of adopting pristine lattices. In this way, these results suggest that the value for D_0 mentioned above is the limit of diffusivity in PTA lattices.

Finally, Fig. 6 shows the temperature-dependent polaron mobility in 1D PTA lattices, which is derived as an average of 1000 realizations for different thermal baths. Setting $N = 1$, we can use Eqs. 3 and 4 to calculate the polaron mobilities. In this sense, the calculated mobilities have the order of magnitude of 10^{-2} cm^2(Vs)$^{-1}$. This order of magnitude agrees with other results presented in the literature[15,16,20,42,43]. Moreover, it is worthwhile to stress that intrinsic charge mobility is difficult to obtain experimentally. Nevertheless, these theoretical results can provide reference values.

Methods

The approach employed here is based on a semiclassical Holstein-Peierls Hamiltonian[35] that is used to describe the polaron dynamics in a one-dimensional PTA lattice with 100 sites and periodic boundary conditions. The model Hamiltonian considered here is a 1D version of the 2D Hamiltonian developed in ref. [31], where each site denotes a PTA molecule that has two degrees of freedom: an intramolecular distortion u_j that represents the internal deformation of a molecule in the crystal and non-local intermolecular v_j displacement that describes the deviation from its equilibrium position (see Fig. 7). In this sense, the model Hamiltonian used here is denoted as

$$H = H_{\text{elec,intra}} + H_{\text{elec,inter}} + H_{\text{latt,intra}} + H_{\text{latt,inter}} \tag{6}$$

where

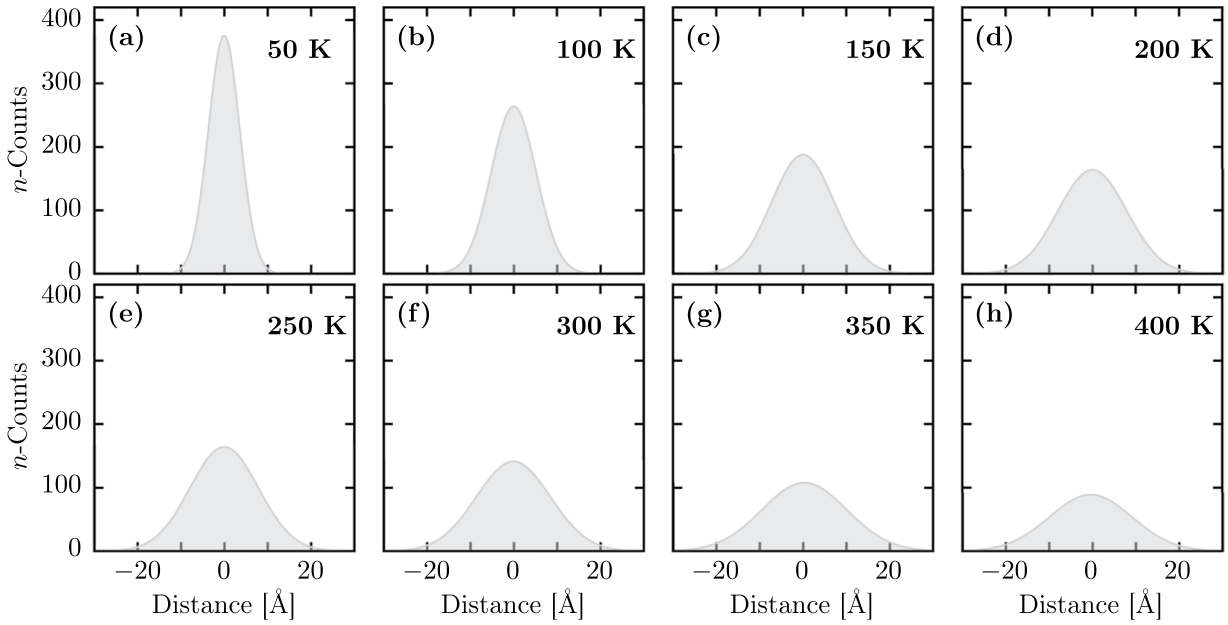

Figure 4. Distribution of the polaron displacement from its origin for the following thermal baths: (**a**) 50 K, (**b**) 100 K, (**c**) 150 K, (**d**) 200 K, (**e**) 250 K, (**f**) 300 K, (**g**) 350 K, and (**h**) 400 K.

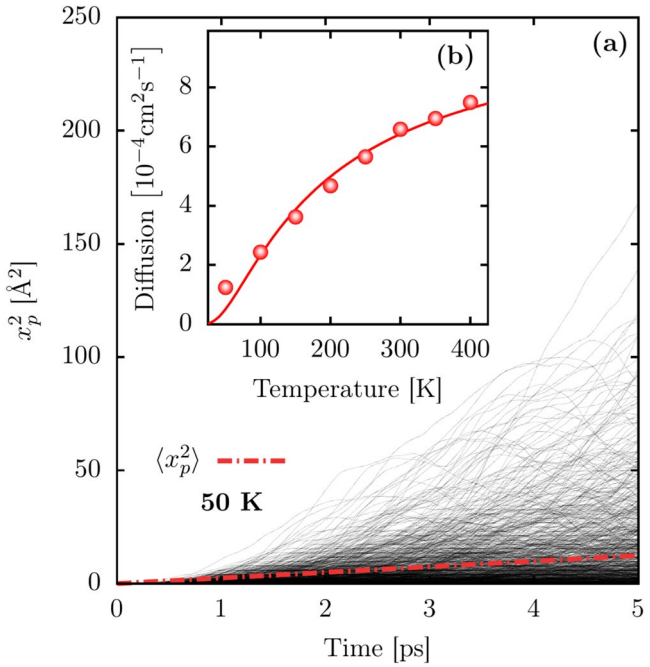

Figure 5. (**a**) Time-dependent squared displacement for the polaron transport in a 1D PTA lattice. (**b**) Temperature-dependent polaron diffusivity.

$$H_{\text{elec,intra}} = \sum_j \alpha_1 u_j \hat{c}_j^\dagger \hat{c}_j \tag{7}$$

and

$$H_{\text{elec,inter}} = \sum_j \left(J_{j,j+1} \hat{c}_{j+1}^\dagger \hat{c}_j + \text{H.C.} \right), \tag{8}$$

with

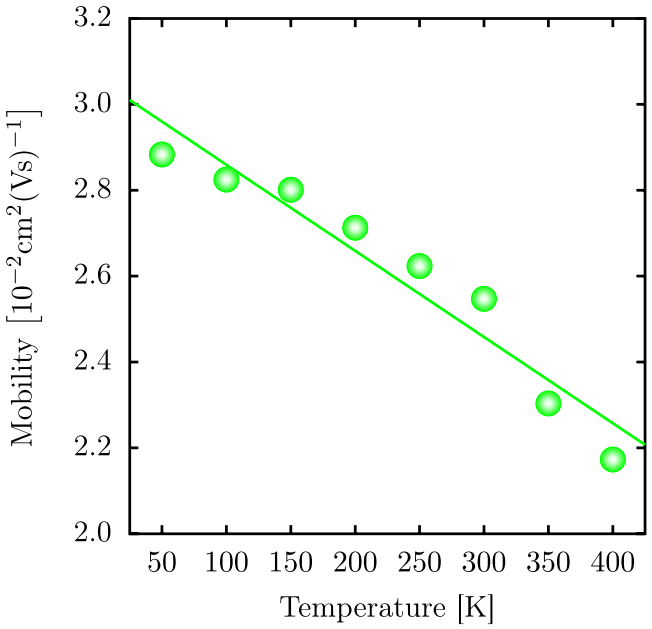

Figure 6. Temperature-dependent polaron mobility. The mobility is derived as an average over 1000 realizations.

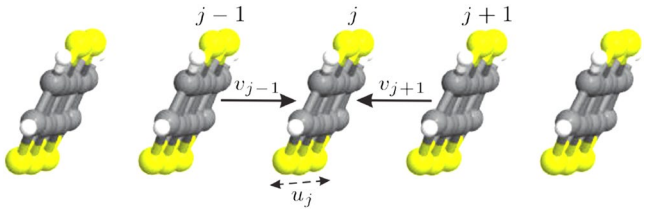

Figure 7. Schematic representation of a one-dimensional PTA chain, where u_j and v_j denote the intra and intermolecular degrees of freedom for a j site, respectively.

$$J_{j,j+1} = J_0 - \alpha_2(v_{j+1} - v_j). \tag{9}$$

J_0 represents the transfer integral for the pristine lattice, α_1 and α_2 denote the intra and intermolecular electron-phonon coupling strengths, and $\hat{c}_j^\dagger$ ($\hat{c}_j$) creates (annihilates) a charge carrier at the j-site.

We use two harmonic oscillators, one for the intra and another one for the intermolecular vibrational modes, to address the lattice degrees of freedom as follows:

$$H_{\text{latt,intra}} = \frac{K_1}{2}\sum_j (u_j)^2 + \frac{M_1}{2}\sum_j (\dot{u}_j)^2 \tag{10}$$

and

$$H_{\text{latt,inter}} = \frac{K_2}{2}\sum_j (v_{j+1} - v_j)^2 + \frac{M_2}{2}\sum_j (\dot{v}_j)^2, \tag{11}$$

where K_1 (K_2) is the force constant and M_1 (M_2) is the harmonic oscillator mass for the intramolecular (intermolecular) degree of freedom.

The electronic dynamics is described by using the time-dependent Schrödinger equation

$$i\hbar\dot{\psi}_j(t) = \sum_{j'} H_{j,j'}(t)\psi_{j'}(t). \tag{12}$$

$H_{j,j'}$ are the Hamiltonian matrix elements and $\psi_j(t)$ represents the electron wave function of the j-site at an instant t.

The lattice motion, in turn, is governed by the Euler-Lagrange Equations

$$\frac{\mathrm{d}}{\mathrm{d}t}\left(\frac{\partial\langle L\rangle}{\partial\dot{\xi}_i}\right)-\frac{\partial\langle L\rangle}{\partial\xi_i}=0. \tag{13}$$

To take into account the lattice effects, it is necessary to obtain the expectation value of the Lagrangean, $\langle\psi|L|\psi\rangle$, where $|\psi\rangle$ is the Slater wave function represented in the second quantization formalism by $|\psi\rangle = a_1^\dagger a_2^\dagger\cdots a_n^\dagger|\rangle$. The Lagrangean is,

$$\begin{aligned} L &= \frac{M_1}{2}\sum_j \dot{u}_j^2+\frac{M_2}{2}\sum_j \dot{v}_j^2-\left(\frac{1}{2}K_1\sum_j u_j^2+\frac{1}{2}K_2\sum_j (v_{j+1}-v_j)^2\right)\\ &\quad+\sum_j \alpha_1 u_j \hat{c}_j^\dagger \hat{c}_j+\sum_j (J_{j,j+1}\hat{c}_{j+1}^\dagger \hat{c}_j+\text{H.C.}) \end{aligned} \tag{14}$$

thus,

$$\begin{aligned} \langle L\rangle &= \frac{M_1}{2}\sum_j \dot{u}_j^2+\frac{M_2}{2}\sum_j \dot{v}_j^2-\left(\frac{1}{2}K_1\sum_j u_j^2+\frac{1}{2}K_2\sum_j (v_{j+1}-v_j)^2\right)\\ &\quad+\sum_j (\alpha_1 u_j+J_0-\alpha_2(v_{j+1}-v_j))\sum_{j,j'}\psi_j(t)\psi_{j'}^*(t), \end{aligned} \tag{15}$$

where ξ are the u, v coordinates for a given site. The sum is realized only for the occupied states. Note also that the last equation is responsible for the connection between the electronic and lattice parts of the system. The Ehrenfest method couples these two separate approximations: the electrons are quantumly described by its time-dependent electron density (a mean-field approximation), whereas classical (Newtonian) mechanics governs the nuclei motion. This mean-field approximation breaks the microscopic correlations between the force experienced by the nucleus due to the electrons and the momentum of the nucleus. The usage of such an approach is well justified in the case of charge transport. Regarding the treatment of the nuclei as classical particles, classical treatment assumes that the number of phonons (intra and inter molecular lattice vibrations) and their related energy (Ep) involved is large, i.e., $Ep \ll K_BT$. Moreover, in the case of thermally activated transport, the classical approach is justified if the activation energy of nuclear coordinates E_A follows the relationship $E_A \ll K_BT$. In this sense, the Newtonian equations are

$$F_u \equiv M_1\ddot{u}_j(t) = -K_1u_j(t)-\alpha_1\rho_{j,j}(t), \tag{16}$$

and

$$\begin{aligned} F_v &\equiv M_2\ddot{v}_j(t)\\ &= -K_2(2v_j(t)-v_j+1(t)-v_j-1(t))\\ &\quad-\frac{\alpha_2}{M_2}(\rho_{j;\,j-1}(t)-\rho_{j+1;\,j}(t)-\rho_{j-1;\,j}(t)+\rho_{j;j+1}(t)), \end{aligned} \tag{17}$$

In the equations above, $\rho_{j,j'}$ is the electronic density matrix, that is defined as follows

$$\rho_{j,j'} = \psi_j(t)\psi_{j'}^*(t). \tag{18}$$

The polaron diffusion in PTA lattices is studied by modifying the approach described in ref. [31], particularly Eqs. 10 and 11 of that work, to include temperature effects. In this sense, a thermal bath is considered in our approach by adding thermal random forces with zero mean value $\langle R(t)\rangle \equiv 0$ and variances

$$\langle R_j^{\text{intra}}(t)R_{j'}^{\text{intra}}(t')\rangle \equiv 2k_BTM_1\lambda_1\delta_{j,j'}\delta(t-t') \tag{19}$$

and

$$\langle R_j^{\text{inter}}(t)R_{j'}^{\text{inter}}(t')\rangle \equiv 2k_BTM_2\lambda_2\delta_{j,j'}\delta(t-t'), \tag{20}$$

to the equations of motion for the lattice backbone, F_u and F_v, within the scope of Langevin formalism. Here, we suppress the indexes x and y, as presented in the equations of ref. [31], since we are considering just the horizontal direction for our model 1D PTA lattice. λ_1 and λ_2 are included in the equations above to keep the temperature constant after a transient period, namely thermalization. Therefore, the new equations of motion for the lattice have the following form

$$F_u' \equiv F_u - M_1\lambda_1\dot{u}_j + R_j^{\text{intra}}(t), \tag{21}$$

and

$$F_v' \equiv F_v - M_2\lambda_2\dot{v}_j + R_j^{\text{inter}}(t). \tag{22}$$

Parameter	Value
J_0	173.0 meV[16,20,53]
α_1	2.0 eV/Å[31]
α_2	0.5 eV/Å[31]
K_1	14.0 eV/Å^2 [31,47]
K_2	0.9 eV/Å^2 [31,47]
M_1	3.2×10^{10} eV (as/Å)^2
M_2	6.4×10^{10} eV (as/Å)^2
a	3.5 Å [15,20]
λ_1	5.0×10^4 as^{-1} [48]
λ_2	5.0×10^4 as^{-1} [48]

Table 1. Set of parameters used in the simulations to study the temperature-dependent polaron dynamics. In the units below, "as" means attosecond.

Equations 21 and 22 are stochastic differential equations (SDEs) and we use the Brünger-Brooks-Karplus (BBK) integrator to solve these SDEs[44,45]. The ground state lattice geometry is obtained using the Resilient back-PROPagation (RPROP) algorithm[46]. The lattice and electronic dynamics are solved within the scope of the Ehrenfest Molecular Dynamics approach, as explained in ref. [31]. Importantly, the Holstein–Peierls approach used here has been successfully used to study oligoacene crystals in previous researches, showing a good track record[35–37,47–52].

Table 1 presents the set of parameters used in the simulations performed here to study the polaron diffusion in 1D PTA lattices. These parameters were obtained from theoretical and experimental studies in the literature[15,16,20,22,53–55]. The temperature regimes range from 50 to 400 K and the oscillator masses M_1 and M_2 (see ref. [31]) are the masses of one and two pentathienoacene molecules, respectively. The units adopted to express the values of these masses in Table 1 are commonly used in Su-Schriffer-Heeger (SSH) based approaches. It is worthwhile to mention that an 1D approach, when it comes to PTA lattices, is a reasonable approximation since this material is highly anisotropic and may present an electronic coupling about 173 meV in one direction and less than 2 meV for the other ones[16].

Received: 2 December 2019; Accepted: 1 April 2020;
Published online: 06 May 2020

References

1. Mazzio, K. A. & Luscombe, C. K. The future of organic photovoltaics. *Chem. Soc. Rev.* **44**, 78–90 (2015).
2. Kippelen, B. & Brédas, J.-L. Organic photovoltaics. *Energy Environ. Sci.* **2**, 251–261 (2009).
3. Klimash, A. *et al*. Intermolecular interactions in molecular crystals and their effect on thermally activated delayed fluorescence of helicene-based emitters. *J. Mater. Chem. C* **6**, 10557–10568 (2018).
4. Yuan, W. Z. *et al*. Efficient solid emitters with aggregation-induced emission and intramolecular charge transfer characteristics: Molecular design, synthesis, photophysical behaviors, and oled application. *Chem. Mater.* **24**, 1518–1528 (2012).
5. Reese, C. & Bao, Z. Organic single-crystal field-effect transistors. *Mater. Today* **10**, 20–27 (2007).
6. Zhou, J. *et al*. Solution-processed and high-performance organic solar cells using small molecules with a benzodithiophene unit. *J. Am. Chem. Soc.* **135**, 8484–8487 (2013).
7. Bagher, A. M. Comparison of organic solar cells and inorganic solar cells. *Int. J. Renew. Sustain. Energy* **3**, 53–58 (2014).
8. Girlando, A. *et al*. Peierls and holstein carrier-phonon coupling in crystalline rubrene. *Phys. Rev. B* **82**, 035208 (2010).
9. Ostroverkhova, O. Organic optoelectronic materials: Mechanisms and applications. *Chem. Rev.* **116**, 13279–13412 (2016).
10. Oberhofer, H., Reuter, K. & Blumberger, J. Charge transport in molecular materials: An assessment of computational methods. *Chem. Rev.* **117**, 10319–10357 (2017).
11. Holstein, T. Studies of polaron motion: Part i. the molecular-crystal model. *Annals physics* **8**, 325–342 (1959).
12. Holstein, T. Studies of polaron motion: Part ii. the "small" polaron. *Annals Phys.* **8**, 343–389 (1959).
13. Stafström, S. Electron localization and the transition from adiabatic to nonadiabatic charge transport in organic conductors. *Chem. Soc. Rev.* **39**, 2484–2499 (2010).
14. Coropceanu, V. *et al*. Charge transport in organic semiconductors. *Chem. reviews* **107**, 926–952 (2007).
15. Zhang, X. *et al*. Theoretical comparative studies on transport properties of pentacene, pentathienoacene, and 6, 13-dichloropentacene. *J. computational chemistry* **36**, 891–900 (2015).
16. Takimiya, K., Nakano, M., Sugino, H. & Osaka, I. Design and elaboration of organic molecules for high field-effect-mobility semiconductors. *Synth. Met.* **217**, 68–78 (2016).
17. Yang, X., Wang, L., Wang, C., Long, W. & Shuai, Z. Influences of crystal structures and molecular sizes on the charge mobility of organic semiconductors: oligothiophenes. *Chem. materials* **20**, 3205–3211 (2008).
18. Nan, G. & Li, Z. Phase dependence of hole mobilities in dibenzo-tetrathiafulvalene crystal: A first-principles study. *Org. Electron.* **13**, 1229–1236 (2012).
19. Stehr, V., Pfister, J., Fink, R., Engels, B. & Deibel, C. First-principles calculations of anisotropic charge-carrier mobilities in organic semiconductor crystals. *Phys. Rev. B* **83**, 155208 (2011).
20. Kim, E.-G. *et al*. Charge transport parameters of the pentathienoacene crystal. *J. Am. Chem. Soc.* **129**, 13072–13081 (2007).
21. Zhang, S.-F., Chen, X.-K., Fan, J.-X. & Ren, A.-M. Charge transport properties in a series of five-ring-fused thienoacenes: A quantum chemistry and molecular mechanic study. *Org. Electron.* **14**, 607–620 (2013).
22. Chai, S., Wen, S.-H., Huang, J.-D. & Han, K.-L. Density functional theory study on electron and hole transport properties of organic pentacene derivatives with electron-withdrawing substituent. *J. computational chemistry* **32**, 3218–3225 (2011).
23. Wang, C., Wang, F., Yang, X., Li, Q. & Shuai, Z. Theoretical comparative studies of charge mobilities for molecular materials: Pet versus bnpery. *Org. Electron.* **9**, 635–640 (2008).

24. Nan, G., Yang, X., Wang, L., Shuai, Z. & Zhao, Y. Nuclear tunneling effects of charge transport in rubrene, tetracene, and pentacene. *Phys. Rev. B* **79**, 115203 (2009).
25. Chen, L., Borrelli, R. & Zhao, Y. Dynamics of coupled electron–boson systems with the multiple davydov d1 ansatz and the generalized coherent state. *The J. Phys. Chem. A* **121**, 8757–8770, https://doi.org/10.1021/acs.jpca.7b07069 (2017).
26. Huang, Z. *et al*. Polaron dynamics with off-diagonal coupling: beyond the ehrenfest approximation. *Phys. Chem. Chem. Phys.* **19**, 1655–1668, https://doi.org/10.1039/C6CP07107D (2017).
27. Zhou, N. *et al*. Fast, accurate simulation of polaron dynamics and multidimensional spectroscopy by multiple davydov trial states. **120**, 1562–1576, https://doi.org/10.1021/acs.jpca.5b12483 (2016).
28. Grossmann, F., Werther, M., Chen, L. & Zhao, Y. Generalization of the davydov ansatz by squeezing. *Chem. Phys.* **481**, 99–107, https://doi.org/10.1016/j.chemphys.2016.04.019 Quantum Dynamics and Femtosecond Spectroscopy dedicated to Prof. Vladimir Y. Chernyak on the occasion of his 60th birthday (2016).
29. Chen, L. & Zhao, Y. Finite temperature dynamics of a holstein polaron: The thermo-field dynamics approach. *The J. Chem. Phys.* **147**, 214102, https://doi.org/10.1063/1.5000823 (2017).
30. Chen, L., Zhao, Y. & Tanimura, Y. Dynamics of a one-dimensional holstein polaron with the hierarchical equations of motion approach. **6**, 3110–3115, https://doi.org/10.1021/acs.jpclett.5b01368 (2015).
31. Junior, M. L. P. *et al*. Polaron properties in pentathienoacene crystals. *Synth. Met.* **253**, 34–39 (2019).
32. Duhm, S. *et al*. Charge reorganization energy and small polaron binding energy of rubrene thin films by ultraviolet photoelectron spectroscopy. *Adv. Mater.* **24**, 901–905 (2012).
33. Gruhn, N. E. *et al*. The vibrational reorganization energy in pentacene: molecular influences on charge transport. *J. Amer. Chem. Soc.* **124**, 7918–7919 (2002).
34. Fröhlich, H. Electrons in lattice fields. *Adv. Phys.* **3**, 325–361 (1954).
35. Junior, L. A. R. & Stafström, S. Polaron stability in molecular semiconductors: theoretical insight into the impact of the temperature, electric field and the system dimensionality. *Phys. Chem. Chem. Phys.* **17**, 8973–8982 (2015).
36. Ribeiro, L. A. & Stafström, S. Impact of the electron–phonon coupling symmetry on the polaron stability and mobility in organic molecular semiconductors. *Phys. Chem. Chem. Phys.* **18**, 1386–1391 (2016).
37. Junior, L. A. R. & Stafström, S. Polaron dynamics in anisotropic holstein–peierls systems. *Phys. Chem. Chem. Phys.* **19**, 4078–4084 (2017).
38. Ribeiro, L. A., da Cunha, W. F., Neto, P. H. O., Gargano, R. & e Silva, G. M. Effects of temperature and electric field induced phase transitions on the dynamics of polarons and bipolarons. *New J. Chem.* **37**, 2829–2836 (2013).
39. de Oliveira Neto, P. H., da Cunha, W. F. & e Silva, G. M. Charge carrier untrapping by temperature effects in conjugated polymers. *Europhys. Lett.* **88**, 67006 (2009).
40. da Cunha, W. F., Ribeiro Junior, L. A., Gargano, R. & e Silva, G. M. Critical temperature and products of intrachain polaron recombination in conjugated polymers. *Phys. Chem. Chem. Phys.* **16**, 17072–17080 (2014).
41. Kadashchuk, A. *et al*. Role of transport band edge variation on delocalized charge transport in high-mobility crystalline organic semiconductors. *Phys. Rev. B* **96**, 125202 (2017).
42. Xiao, K. *et al*. A highly p-stacked organic semiconductor for field-effect transistors based on linearly condensed pentathienoacene. *J. Am. Chem. Soc.* **127**, 13281–13286 (2005).
43. Kuo, M.-Y. & Liu, C.-C. Molecular design toward high hole mobility organic semiconductors: tetraceno [2, 3-c] thiophene derivatives of ultrasmall reorganization energies. *The J. Phys. Chem. C* **113**, 16303–16306 (2009).
44. Brünger, A., Brooks, C. L. & Karplus, M. Stochastic boundary conditions for molecular dynamics simulations of st2. *water. Chem. physics letters* **105**, 495–500 (1984).
45. Izaguirre, J. A., Catarello, D. P., Wozniak, J. M. & Skeel, R. D. Langevin stabilization of molecular dynamics. *The J. chemical physics* **114**, 2090–2098 (2001).
46. Riedmiller, M. & Braun, H. A direct adaptive method for faster backpropagation learning: The rprop algorithm. In *Neural Networks, 1993., IEEE International Conference on*, 586–591 (IEEE, 1993).
47. Pereira Júnior, M. L., de Sousa Junior, R. T., e Silva, G. M. & Ribeiro Junior, L. A. Stationary polaron properties in organic crystalline semiconductors. *Phys. Chem. Chem. Phys.* **21**, 2727–2733 (2019).
48. Junior, M. L. P. & Junior, L. A. R. Polaron dynamics in oligoacene stacks. *J. molecular modeling* **23**, 257 (2017).
49. Junior, M. L. P. & Junior, L. A. R. Polaron stability in oligoacene crystals. *J. molecular modeling* **23**, 89 (2017).
50. Mozafari, E. & Stafström, S. Polaron stability in molecular crystals. *Phys. Lett. A* **376**, 1807–1811 (2012).
51. Mozafari, E. & Stafström, S. Polaron dynamics in a two-dimensional holstein-peierls system. *The J. chemical physics* **138**, 184104 (2013).
52. Pereira, M. L., de Sousa, R. T., e Silva, G. M. & Ribeiro, L. A. Modeling polaron diffusion in oligoacene-like crystals. *The J. Phys. Chem. C* **123**, 4715–4720 (2019).
53. Huang, J.-D., Wen, S.-H. & Han, K.-L. First-principles investigation of the electronic and conducting properties of oligothienoacenes and their derivatives. *Chem. – An Asian J.* **7**, 1032–1040 (2012).
54. Yamada, K. *et al*. Single-crystal field-effect transistors of benzoannulated fused oligothiophenes and oligoselenophenes. *Appl. physics letters* **90**, 072102 (2007).
55. Malavé Osuna, R. *et al*. Oxidation of end-capped pentathienoacenes and characterization of their radical cations. *Chem. –A Eur. J.* **15**, 12346–12361 (2009).

Acknowledgements

The authors gratefully acknowledge the financial support from Brazilian Research Councils CNPq, CAPES, and FAPDF and CENAPAD-SP for providing the computational facilities. L.A.R.J. and W.F.G. gratefully acknowledge, respectively, the financial support from FAP-DF grants 0193.001.511/2017 and 00193.0000248/2019-32. L.A.R.J. gratefully acknowledges the financial support from CNPq grant 302236/2018-0. R.T.S.J. gratefully acknowledge, respectively, the financial support from CNPq grant 465741/2014-2, CAPES grants 23038.007604/2014-69 and 88887.144009/2017-00, and FAP-DF grants 0193.001366/2016 and 0193.001365/2016. The authors also would like to thank the support of CAPES (grants 23038.007604/2014-69 FORTE and 88887.144009/2017-00 PROBRAL), CNPq (grants 312180/2019-5 PQ-2, BRICS2017-591 LargEWiN, and 465741/2014-2 INCT in Cybersecurity) and FAP-DF (grants 0193.001366/2016 UIoT and 0193.001365/2016 SSDDC), as well as the cooperation project with the Institutional Security Office of the Presidency of the Republic (grant ABIN 002/2017).

Author contributions

L.A.R.J. and M.L.P.J. were responsible for developing the code. M.L.P.J., W.F.G. ran the calculations. M.L.P.J. and R.T.S.J. built the graphics. L.A.R.J., M.L.P.J., and R.T.S.J. interpreted the results and wrote the paper. All the authors were responsible for discussing the results.

Competing interests
The authors declare no competing interests.

Additional information
Correspondence and requests for materials should be addressed to L.A.R.J.

Reprints and permissions information is available at www.nature.com/reprints.

Publisher's note Springer Nature remains neutral with regard to jurisdictional claims in published maps and institutional affiliations.